14 Light Scattering by Fractal Aggregates

C. M. Sorensen

CONTENTS

14.1 INTRODUCTION

Particulate matter, such as aerosols, are a nonequilibrium state that with time evolves, via aggregation, to form larger particles. Aggregation with coalescence, like one might observe in a cloud of water droplets, leads to bigger, dense particles. Aggregation without coalescence, like one might observe in a cloud of solid, carbonaceous soot particles, leads to bigger, ramified (as opposed to

dense) particles. Three decades ago, we learned that these ramified aggregates could be quantitatively described as fractal aggregates.[1]

Fractal aggregates are very common in both natural and technical settings. Perhaps the most common is soot from various combustion processes that occur on the face of the Earth, due to either human or natural activity. Other examples include any solid particle aerosol that has been allowed sufficient time for the aggregation processes to have effect, such as fumed SiO_2.

The purpose of this chapter is to review the light-scattering properties of fractal aggregates. Since fractal aggregates are common, we desire to know and understand their physical properties; and light scattering is an important physical characteristic. With light scattering we can study or monitor aggregation kinetics in the lab or in industrial settings. Light scattering is also very important for understanding the effects of aerosols on the Earth's climate. In 2001, this author presented a review of light scattering by fractal aggregates.[2] Another review of how fractal aggregates scatter light, that contains some of the material covered in the previous review but to a lesser extent, is presented here. This new review also includes advances made in the intervening nine years.

14.2 FRACTAL AGGREGATES

Fractals are scale invariant objects. This means that they appear the same upon a change of scale; they are self-similar. Once we were taught how to look for fractal aggregates by Mandelbrot,[3] we have come to realize that they abound in nature. Examples include trees, coastlines, mountain ranges, clouds and the subject of this chapter, fractal aggregates.

Fractal aggregates are clusters of particles with a self-similar structure over a finite range of length scales. The particles composing the aggregates are called "primary particles" or "monomers." Ideally, they are spherical with point contacts, but this description is an approximation. Regardless, we take their radius as a, and this sets the lower limit to the fractal scaling range. The upper limit is well described by the radius of gyration R_g, which is a root-mean-square radius that quantifies the overall size of the aggregate. A consequence of self-similarity is that the number of primary particles N in the aggregate scales as a power law with the reduced size of the aggregate as

$$N = k_0 \left(\frac{R_g}{a} \right)^{D_f} \tag{14.1}$$

In Equation 14.1, D_f is the fractal dimension and k_0 is the scaling prefactor. Equation 14.1 may be considered as the defining relation for fractal aggregates. One can say that the "mass" N scales with the linear size R_g with the dimensionality D_f, which is typically a noninteger. Figure 14.1 shows an ensemble of fractal aggregates captured from a flame–soot aerosol. Figure 14.2 shows a schematic drawing of a fractal aggregate illustrating Equation 14.1.

A second consequence of scale invariant self-similarity is that the pair correlation function of the primary particles is a power law that can be expressed as

$$g(r) \sim r^{D_f - d}\, h\left(\frac{r}{R_g} \right) \tag{14.2}$$

Here d is the spatial dimension and $h(x)$ is the cutoff function that describes how the aggregate ends at its perimeter. To preserve the power law, $h(x) = 1$ for $x \ll 1$, and to cut-off the power law, $h(x)$ must decrease faster than any power law for $x \gg 1$. Such a function that has proven to be adequate for fractal aggregates is the stretched exponential

$$h(x) = \exp(-x^{\gamma}) \tag{14.3}$$

FIGURE 14.1 Soot fractal aggregates with fractal dimension $D_f = 1.78 \pm 0.07$.

Various studies have shown that $\gamma \sim 2$–2.5 (see refs. [4]–[7]). Aerosol particles almost always aggregate via random Brownian motion; aggregates meeting and sticking together. Such a process is called diffusion limited cluster aggregation (DLCA).[8,9] In three-dimensional space, DLCA leads to fractal aggregates with $D_f = 1.78 \pm 0.1$ and $k_0 = 1.3 \pm 0.2$.[10–12] These numbers can be considered universal, since they have been determined from experiments on both aerosols and colloids, from simulations, which show an underappreciated anticorrelation between the fit values of D_f and k_0,[12] and a simple analytical theory.[13] The prefactor k_0 for some combustion aerosols has been measured

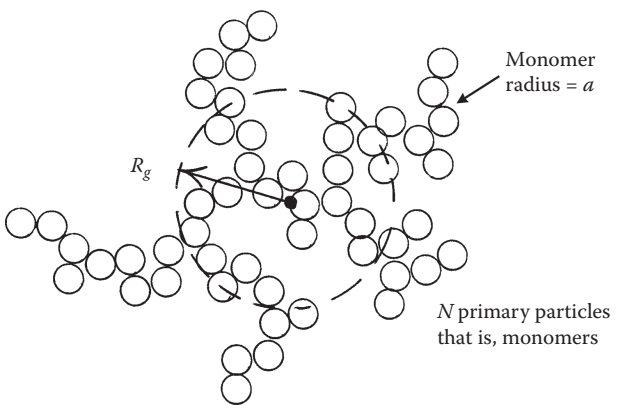

FIGURE 14.2 Schematic diagram of a fractal aggregate showing the monomer or primary particle size, a, the aggregate radius of gyration, R_g, and the number of monomers, N.

to be as large as 2.5[14] and this possible break from universality appears legitimate and warrants more attention. There also are situations where aggregates are found with larger fractal dimensions as a result of processes following the aggregation processes, such as shear restructuring or cloud processing. More recently, hybrid superaggregates with $D_f = 1.8$ on short length scales and $D_f = 2.6$ on larger length scales have been discovered.[15–17]

In colloids, the probability of cluster–cluster sticking upon meeting can be made very small and then a new type of aggregation ensues, reaction limited cluster aggregation (RLCA). Although RLCA is common in colloids, it does not seem to have been observed in aerosols. RLCA leads to $D_f = 2.05$–2.15 with $k_0 = 0.94$ for the lower value.[7]

14.3 LIGHT SCATTERING

14.3.1 Polarization

The polarization of light is the direction of its electric field vector. Maxwell's laws enforce that this is perpendicular to the direction of propagation; hence, there are two independent polarizations. Natural light that is emitted by the sun, light bulbs, and so on. have equal amounts of each of these two independent polarizations. Such light is sometimes called "unpolarized" or "randomly" polarized. Lasers are very often, but not always, polarized. A typical laboratory setup positions a laser shining its beam in the horizontal direction with the polarization in the vertical direction.

To understand the effect of scattering on polarization, consider a light wave traveling in the positive z direction incident upon a particle at the origin as drawn in Figure 14.3. The propagation direction is described by the incident wave vector $\vec{k}_i$ with magnitude $|\vec{k}_i| = 2\pi/\lambda$ where λ is the wavelength of the light in the medium. The incident light is polarized along the vertical x axis. The y–z plane is horizontal and is called the "scattering plane." Light is scattered in the direction of the scattered wave vector $\vec{k}_s$. We consider only elastic scattering; hence,

$$|\vec{k}_s| = |\vec{k}_i| \tag{14.4}$$

Because these magnitudes are equal, we represent each simply by k.

For particles small compared to the wavelength, the polarization of the scattered light is in the direction of the projection of the incident polarization at the particle, which is in the direction $\hat{x}$, onto a plane perpendicular to $\vec{k}_s$, plane p in Figure 14.3. In vector notation, this is equivalent to

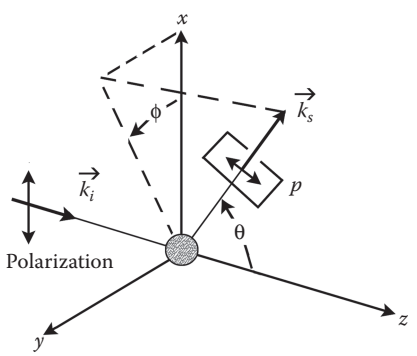

FIGURE 14.3 Geometry of scattering for an incident light wave traveling along the positive z-axis with propagation direction defined by the incident wave vector k_i and with polarization in the vertical x direction. Light is scattered from the small, spherical particle to the detector in the direction of the scattering wave vector k_s. The scattered polarization is in the direction of the projection of the incident polarization at the scatterer onto the plane p, which is perpendicular to the detector direction k_s.

the double cross product, $(\hat{k}_s \times \hat{x}) \times \vec{k}_s$, where $\hat{k}_s$ is the unit vector in the scattering direction. With either the projection or the double cross product, it can be shown that the scattered intensity obeys the proportionality

$$I_{\text{sca}} \propto 1 - \cos^2 \phi \sin^2 \theta. \tag{14.5}$$

Most laboratory experiments are confined to the scattering plane; hence, $\phi = 90°$. Then the angle θ is the scattering angle; $\theta = 0$ is forward scattering. An incident vertical polarization projects completely onto plane *p* of Figure 14.3 with no angular dependence. This is corroborated by Equation 14.5 with $\phi = 90°$. Horizontally polarized incident light would scatter out with horizontal polarization with intensity proportional to $\cos^2 \theta$, shown in Equation 14.5. Randomly polarized light would be a simple linear combination of these two polarizations weighted by their intensities.

14.3.2 Cross Sections

Cross sections describe the extent of scattering. As the name implies, their units always include an area (m^2). The concept is that the cross section for scattering is the effective area the incident wave sees and hence, blocks its path. The result of this blocking is either scattering, absorption, or both.

14.3.2.1 The Differential Scattering Cross Section

The differential scattering cross section describes the power scattered, P_{sca}(W), in a given direction. The direction has a small spread in angles, a differential of a solid angle, $d\Omega$ (steradian). For an incident irradiance (often called wrongly as the intensity) I_o (W/m^2), the power scattered per solid angle is

$$\frac{P_{\text{sca}}}{\Omega} = \frac{dC_{\text{sca}}}{d\Omega} I_o \tag{14.6}$$

In Equation 14.6, $dC_{\text{sca}}/d\Omega$ is the differential scattering cross section with units of m^2/steradian.

The scattered irradiance is the scattered power per unit area of detection

$$I_{\text{sca}} = P_{\text{sca}}/A \tag{14.7}$$

The solid angle subtended by the detector a distance *r* from the scatterer is

$$\Omega = A/r^2 \tag{14.8}$$

Thus, from Equations 14.6–14.8, we obtain

$$I_{\text{sca}} = I_o \frac{dC_{\text{sca}}}{d\Omega} \frac{1}{r^2} \tag{14.9}$$

This equation contains the well-known $1/r^2$ dependence due to the three-dimensional geometry of space.

14.3.2.2 The Total Scattering Cross Section

The total scattering cross section describes the total scattering in all directions. Thus, it is found by the integration of the differential cross section over the complete solid angle

$$C_{\text{sca}} = \int_{4\pi} \frac{dC_{\text{sca}}}{d\Omega} d\Omega \tag{14.10}$$

The units of C_{sca} are m^2. This integral must include polarization effects (see above). The differential element $d\Omega$ in three-dimensional Euclidean space is

$$d\Omega = d\cos(\theta)\, d\varphi \tag{14.11}$$

(See Figure 14.3 for the definition of the polar coordinates θ and ϕ.) The total power scattered from the incident beam of irradiance I_0 is

$$P_{sca} = I_0\, C_{sca}. \tag{14.12}$$

14.3.3 The Rayleigh–Debye–Gans Approximation

The exact description of light scattering from any particle requires solution of the Maxwell equations for the interaction of the electromagnetic wave with that particle. Perhaps the best known example of this is the Lorenz–Mie solution for scattering from a dielectric sphere.[18–20] Maxwell's equations are applied to the particular case of spherical boundary conditions to yield an infinite series of special functions related to that symmetry. Such an approach is useless for fractal aggregates, because the aggregate has no such symmetry.

Lessons can be learned, however, from the Lorenz–Mie solution. Studies from this laboratory[21–24] have shown that the Lorenz–Mie solution is based on simple diffraction from the sphere. Alternately, diffraction is the result of the wave nature of light and scattering is a result of both diffraction and the electromagnetic interaction of the light with the particle. If that electromagnetic interaction is small, diffraction dominates. The criterion for diffraction to dominate is that the so-called phase-shift parameter, ρ, defined as

$$\rho = 2kR(m - 1), \tag{14.13}$$

is less than one. In Equation 14.13, k is the wave number and equals $2\pi/\lambda$, where λ is the light wavelength, R is the radius of the particle and m is the particle's refractive index. Use of the diffraction result to describe light scattering is often called the Rayleigh–Debye–Gans (RDG) approximation.

The RDG approximation can be made somewhat tenable for fractal aggregates with the following argument.[2] We can consider an aggregate as a dispersion of the primary particle optical material in vacuum. We then apply the Maxwell–Garnet effective medium theory, which is good for low and uniform density dispersions. The second condition is not satisfied by fractal aggregates, but remembering this caveat, we proceed. The Maxwell–Garnet theory allows one to calculate the effective index of refraction of the average medium that is composed of the primary particles and the vacuum as

$$(m - 1)_{eff} = f_v(m - 1). \tag{14.14}$$

For a fractal aggregate, the volume fraction of monomers is approximately

$$f_v = \frac{Na^3}{R_g^3}. \tag{14.15}$$

This combined with the fundamental equation for fractal aggregates, Equation 14.1, yields

$$(m - 1)_{eff} = R_g^{D_f - 3} a^{3 - D_f}\ (m - 1) \tag{14.16}$$

where we set $k_0 = 1$. Substitution of Equations 14.13 into 14.16 finds the fractal aggregate phase-shift parameter as

$$\rho = 2kR_g^{D_f - 2} a^{3 - D_f}\ (m - 1) \tag{14.17}$$

For a given optical wave number k and monomer of size a and refractive index m, Equation 14.17 shows that for $D_f < 2$ the phase-shift parameter gets *smaller* with increasing aggregate size. Thus, the condition for RDG to hold can be ultimately satisfied. On the other hand, for $D_f > 2$ increasing R_g increases the cluster phase-shift parameter, taking it further away from the regime in which the RDG theory can be successful. Equation 14.17 must be viewed with some caution because of the misuse of the Maxwell–Garnet theory.

14.4 THE STRUCTURE FACTOR

14.4.1 The Scattering Wave Vector

We consider a scalar electromagnetic wave incident upon a scattering element, or scatterer, at $\vec{r}$ as shown in Figure 14.4. We choose a scalar wave, because the development that follows is not affected by polarization. We make the scatterer point-like so that it scatters isotropically throughout space. The incident field at $\vec{r}$ in complex notation is

$$E(\vec{r}) = E_0 \exp(i\vec{k}_i \cdot \vec{r}) \tag{14.18}$$

where $i = \sqrt{-1}$ and $\vec{k}_i$ is the incident wave vector. The field scatters toward the detector, at $\vec{R}$, in the direction $\vec{k}_s$, the scattered wave vector. Under the assumption of elastic scattering, Equation 14.4, the field at the detector is

$$E(\vec{R}) \sim E(r)\exp(i\vec{k}_s \cdot (\vec{R} - \vec{r})) \tag{14.19}$$

Substitution of Equation 14.18 yields

$$E(R) \sim E_0 \exp(i\vec{k}_s \cdot \vec{R})\exp(i(\vec{k}_i - \vec{k}_s) \cdot \vec{r}) \tag{14.20}$$

We have dropped the equality for the proportionality, because we do not know and do not need to know the strength of the scattering element at $\vec{r}$. The second term of Equation 14.20 shows that the phase at the detector is a function of the position of the scattering element and the vector

$$\vec{q} = \vec{k}_i - \vec{k}_s \tag{14.21}$$

This vector $\vec{q}$ is called the *scattering wave vector.* Its direction is in the scattering plane from k_s to $\vec{k}_i$, as shown in Figure 14.5. Figure 14.5, the elasticity condition Equation 14.4, and simple

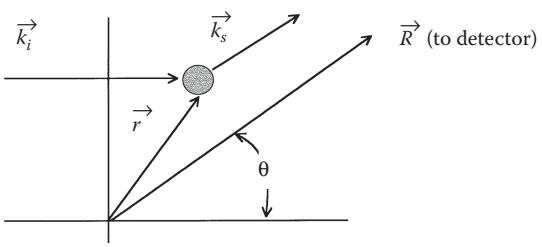

FIGURE 14.4 Diagram of an incident wave with propagation wave vector $\vec{k}_i$ scattering from a point-like scatterer at $\vec{r}$ the scattered wave leaves $\vec{r}$ in the direction of $\vec{k}_i$, the scattered wave vector, toward the detector at great distance $\vec{R}$.

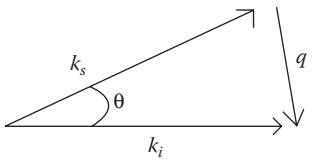

FIGURE 14.5 The scattering wave vector and its association with and the scattering angle θ.

trigonometry yield the magnitude of q to be

$$q = 2k \sin(\theta/2) \tag{14.22a}$$

$$= (4\pi/\lambda) \sin(\theta/2) \tag{14.22b}$$

where θ is the scattering angle.

The importance of q is that it describes how the phase at the detector, whatever that might be, depends on the position of the scatterer and the angle of scattering. Our approach below involves envisioning any scattering object, as composed of a great many point-like scatterers at various $\vec{r}$. The object is represented as a system of scatterers.[25] An important characteristic of q is that its inverse, q^{-1}, represents the length scale, or the probe length, of the scattering experiment. This follows from the second term in Equation 14.20, which can now be written as

$$E_{\text{sca}}(\vec{q}, \vec{r}) \sim E_0 \exp(i\vec{q} \cdot \vec{r}) \tag{14.23}$$

where E_{sca} is the amplitude of the scattered wave. Equation 14.23 shows that if the variation of r is small compared to q^{-1}, the scattered field does not significantly change; whereas if r varies greatly relative to q^{-1}, the scattered field changes significantly. Thus, q^{-1} represents a length scale to be compared to length scales of the scatterer; this comparison determines the scattered field.

14.4.2 The Fundamental Equation for the Structure Factor

To determine the scattering from a material object of finite extent, we consider that object to be composed of a multitude of point-like scatterers. We call this concept a "system of scatterers."[25] Here we assume that the object meets the RDG criterion. Then, the scattering from each individual scatterer of the object is so weak that they do not sense each other's scattered fields. Hence, each scatterer sees only the incident field. Each scatterer then sends (scatters) a wave out to the detector with phase information given by Equation 14.23. Then the total field at the detector due to the system of N scatterers is the sum over N scatterers

$$E(q) \sim E_0 \sum_i^N \exp(i\vec{q} \cdot \vec{r}_i) \tag{14.24}$$

Then the intensity of the scattered wave is the square of the amplitude, which for complex amplitudes is the product of the amplitude and its complex conjugate

$$I(q) \sim E_0^2 \sum_i^N \exp(i\vec{q} \cdot \vec{r}_i) \sum_j^N \exp(-i\vec{q} \cdot \vec{r}_j) \tag{14.25}$$

Since we must often deal with ensembles of scatterers with random orientations, we have dropped the vector notation on the left-hand side of Equation 14.25.

The structure factor, $S(q)$, is proportional to the scattered intensity $I(q)$ and defined with the normalization $N^{-2}I(q)$; thus

$$S(q) = N^{-2}\sum_{i}^{N}\sum_{j}^{N}\exp(i\vec{q}\cdot(\vec{r}_i - \vec{r}_j)) \tag{14.26}$$

We regain the equality, because this defines the structure factor.* This normalization ensures $S(0) = 1$.

To convert the sums to integrals in Equation 14.26, we write the density function of the system of scatterers as

$$n(\vec{r}) = \sum_{i}^{N}\delta(\vec{r} - \vec{r}_i) \tag{14.27}$$

where $\delta(\vec{r})$ is the Dirac delta function. Then

$$\sum_{i}^{N}\exp(i\vec{q}\cdot\vec{r}) = \int\exp(i\vec{q}\cdot\vec{r})n(\vec{r})\,\mathrm{d}\vec{r} \tag{14.28}$$

From this and Equation 14.26 we write the structure factor as

$$S(q) = N^2\iint n(\vec{r})n(\vec{r}')\exp(i\vec{q}\cdot(\vec{r} - \vec{r}'))\,\mathrm{d}\vec{r}\,\mathrm{d}\vec{r}' \tag{14.29}$$

Changing variables to $\vec{r}$ and $\vec{u} = \vec{r} - \vec{r}'$ we obtain

$$S(q) = \iint n(\vec{r})n(\vec{r} - \vec{u})\exp(i\vec{q}\cdot\vec{u})\,\mathrm{d}\vec{r}\,\mathrm{d}\vec{u} \tag{14.30}$$

Now recognize that the integral over $\vec{r}$ is a convolution of the density with itself, which we write as

$$g(\vec{u}) = \int n(\vec{r})n(\vec{r} - \vec{u})\,\mathrm{d}\vec{r} \tag{14.31}$$

Then

$$S(q) = \int g(\vec{u})\exp(i\vec{q}\cdot\vec{u})\,\mathrm{d}u \tag{14.32}$$

We find that the structure factor is the Fourier transform of the self convolution of the object's density function.

The function $g(\vec{u})$ of Equations 14.31 and 14.32 is well known in the scattering literature[27–29] and beyond, not so much as the self convolution but as the density autocorrelation function of the object. This function answers the question of how the density correlates with itself. It is a joint probability which, given a scatterer at an arbitrary position, determines the probability of finding another scatterer a position u away. Its importance transcends scattering theory and for condensed matter includes the thermodynamics of the system. Equation 14.32 implies that $S(q)$ and $g(u)$ are Fourier transform pairs.

Under the assumption of isotropy, $S(\vec{q}) = S(q)$ and $g(\vec{u}) = g(u)$, and the solid angle integration can be performed on Equation 14.32 to yield

$$S(q) = 4\pi\int g(u)[(\sin qu)/qu]u^2\,\mathrm{d}u \tag{14.33}$$

* Some authors use a N^{-1} normalization to define $S(q)$.

14.4.2.1 Small *q* Behavior of the Structure Factor: The Guinier Regime

The sine function in the integrand of Equation 14.33 can be expanded for small qu. Then Equation 14.33 becomes two integrals, the first of which is unity by the normalization of $g(u)$, so that we obtain

$$S(q) \approx 1 - \frac{q^2}{6} \int u^2 g(u)\, \mathrm{d}u \tag{14.34}$$

One can show that the radius of gyration for an object is given by

$$R_g^2 = \frac{1}{2} \int u^2 g(u)\, \mathrm{d}u \tag{14.35}$$

Thus,

$$S(q) \approx 1 - \frac{1}{3} q^2 R_g^2. \tag{14.36}$$

Equation 14.36 is the Guinier equation,[26] good in the regime $qR_g < 1$ for all shapes. It is very useful for measuring particle size as described by the radius of gyration. The radius of gyration is a root-mean-square radius. For a sphere $R_g = \sqrt{3/5}R$.

14.4.3 The Structure Factor for Fractal Aggregates

Substitution of the correlation function for fractal aggregates, Equations 14.2 and 14.3, into Equation 14.33 yields the structure factor for fractal aggregates. The key question is what is the value of the exponent γ in the cut-off function? Much of the older literature assumes $\gamma = 1$, that is, an exponential cut-off.[27,28] With this, one finds

$$S(q) = \frac{\sin[(D_f - 1)\, \tan^{-1}(q\xi)]}{(D_f - 1)\, q\xi (1 + q^2\xi^2)^{(D_f - 1)/2}} \tag{14.37}$$

where

$$\xi^2 = \frac{2R_g^2}{D_f (D_f + 1)} \tag{14.38}$$

When $D_f = 2$, the exponential structure factor simplifies to the Fisher–Burford[29] form

$$S(q) = \left(1 + \frac{2q^2 R_g^2}{3D_f} \right)^{-D_f/2} \tag{14.39}$$

This remains a good approximation when $D_f \approx 2$, such as 1.8 or 2.1 as found for DLCA and RLCA, respectively. Because of its simplicity, the Fisher–Burford form has been used a lot; but it is wrong. Surprisingly, it fits data from polydisperse systems well, under the assumption of no polydispersity of the aggregates. This is erroneous; aggregates form due to aggregation, which leads to polydispersity. More correct fits are obtained with more correct structure factors integrated over the polydispersity[30] as described below.

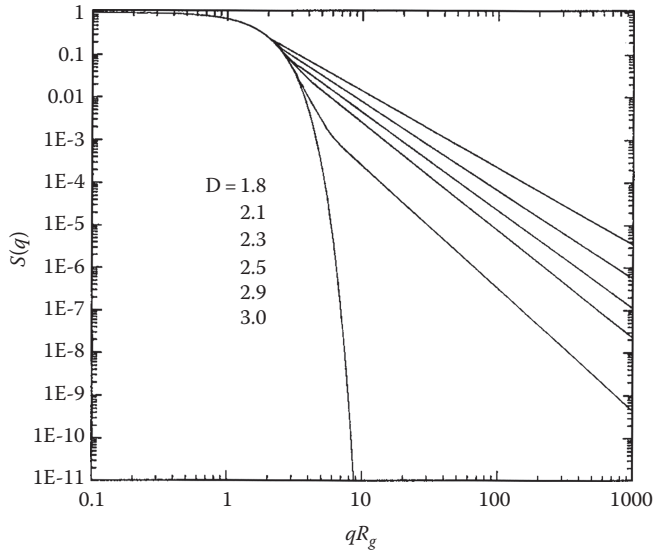

FIGURE 14.6 Double log plot of the structure factor for an aggregate with a Gaussian cut off for its density correlation function.

Current science[4–7] supports a Gaussian cut-off with $\gamma = 2$ as a better descriptor of the fractal correlation function. Then

$$S(\mathrm{q}) = {}_1F_1\left[\frac{D_f}{2},\ \frac{3}{2};\ -\frac{(qR_g)^2}{D_f}\right] \tag{14.40}$$

where ${}_1F_1$ is the Kummer or hypergeometric function. Figure 14.6 shows a plot of the Gaussian structure factor for different D_f values.[2] Note the small hump near $qR_g \approx 2$.

14.5 LIGHT-SCATTERING CROSS SECTIONS

14.5.1 Rayleigh Scattering

We assume that the monomers (primary particles) are Rayleigh scatterers. The conditions for Rayleigh scattering are[18–20]

$$ka < 1 \tag{14.41a}$$

$$|m|\, ka < 1 \tag{14.41b}$$

In Equation 14.41b $m = n + \mathrm{i}k$ is the complex refractive index of the particle. If we deal with optical wavelengths of say $\lambda = 500$ nm and reasonable refractive indices, these conditions imply a particle radius of $a < 80$ nm. The Rayleigh differential scattering cross section for the particle is

$$\frac{\mathrm{d}C_{\mathrm{sca}}}{\mathrm{d}\Omega} = k^4 a^6 F(m) \tag{14.42}$$

where

$$F(m) = \left|\frac{(m^2 - 1)}{(m^2 + 2)}\right|^2 \tag{14.43}$$

Absorption in the RDG regime is given by

$$C_{\text{abs}} = 4\pi k a^3 E(m) \tag{14.44}$$

where

$$E(m) = \text{Imag}\left[\frac{(m^2-1)}{(m^2+2)}\right] \tag{14.45}$$

Imag means to take the imaginary part.

14.5.2 Fractal Aggregate Light-Scattering Cross Sections

Under the RDG approximation, the individual monomers of the fractal aggregate act as point scatterers. Thus, they are the scatterers in our system of scatterers, above. Since they do not interact, the total scattering from the aggregate is determined by the cross section of each individual monomer adding with the others with the proper accounting for the phase differences of the scattered waves from each particle at the detector. This proper accounting is taken care of by the structure factor; recall the structure factor contained solely and completely in the phase information.

14.5.2.1 Fractal Aggregate Differential Scattering Cross Section

The total differential cross section for a fractal aggregate of Rayleigh primary particles under the RDG approximation is

$$\frac{\mathrm{d}C_{\text{sca}}^{\text{agg}}}{\mathrm{d}\Omega} = N^2 \frac{\mathrm{d}C_{\text{sca}}^{\text{m}}}{\mathrm{d}\Omega} S(q) \tag{14.46}$$

where "agg" and "m" mean "aggregate" and "monomer," respectively.

This result is sketched in Figure 14.7 as the scattered intensity, which is directly proportional to the differential cross section, as a function of q on a double logarithmic plot. There we see a q independent Rayleigh regime at small q with an N^2 dependence on the number of monomers in the aggregate. In this regime, the length scale of the scattering process q^{-1} is too big to see the aggregate as anything but an unresolved blob. As q increases to $q \sim R_g^{-1}$, $I(q)$ starts to decline as the Guinier

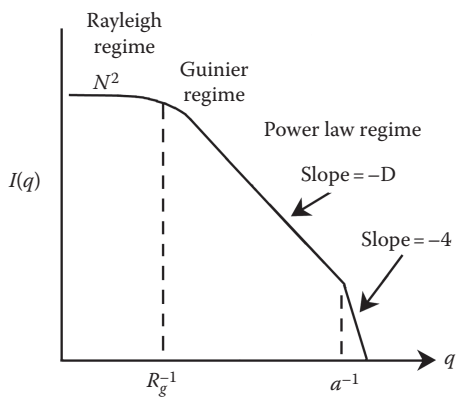

FIGURE 14.7 Double log plot of the scatter light intensity as a function of q for a fractal aggregate made of N spherical particles of radius a. The aggregate has a radius of gyration of R_g and a fractal dimension D_f.

regime is entered. Note, this is when q^{-1} is small enough to begin to resolve the overall aggregate size. It is in this regime that the size of the aggregate can be measured. As q increases further, the power-law regime is entered described by

$$I(q) \sim C(qR_g)^{-D_f} \tag{14.47}$$

Thus, the slope of the log–log plot is $-D_f$ and this provides an opportunity for measurement of the fractal dimension. The best value for the coefficient is $C = 1.0 \pm 0.1$.[2] Finally, a second bend is found at $q \sim a^{-1}$, where the scattering begins to resolve the monomer size, a. Thereafter, the slope is typically −4, the Porod scattering from a sphere.[31,32]

14.5.2.2 Fractal Aggregate Absorption Cross Section

For absorption, the particle independence and nonmultiple scattering conditions of RDG imply the simple result

$$C_{\text{abs}}^{\text{agg}} = NC_{\text{abs}}^{\text{m}} \tag{14.48}$$

The absorption of the aggregate is just the sum of the independent absorptions of its monomers.

14.5.2.3 Fractal Aggregate Total Scattering Cross Section

The total scattering cross section is formally related to the differential cross section by Equation 14.10. The integral must account for the polarization. Under the RDG approximation, the polarization law for the aggregate is the same as it is for the monomers of which it is composed. Then for the common experimental situation of light vertically polarized relative to the scattering plane, the factor of Equation 14.5 must be included to yield

$$C_{\text{sca}} = \iint \frac{\mathrm{d}C_{\text{sca}}}{\mathrm{d}\Omega} \; (1 - \cos^2 \varphi \, \sin^2 \theta) \, \mathrm{d}(\cos\theta) \, \mathrm{d}\varphi \tag{14.49}$$

Substitution of the expression for the differential cross section of a fractal aggregate, Equation 14.46, leads to an integral over the structure factor, which leads to algebraically elaborate results. Instead, we follow the simpler approach of Dobbins and Megaridis[33] who used the small qR_g, Guinier form, universal to all structure factors, and a generalization based on the Fisher–Burford structure factor to obtain

$$C_{\text{sca}}^{\text{agg}} = N^2 C_{\text{sca}}^{\text{m}} G(kR_g), \tag{14.50}$$

where

$$C_{\text{sca}}^{\text{m}} = \frac{8\pi}{3k^4a^6} F(m), \tag{14.51}$$

the Rayleigh total scattering cross section for a sphere of radius a, and

$$G(kR_g) = \left[1 + (4/3D_f)k^2R_g^2\right]^{-D_f/2} \tag{14.52}$$

Dobbins and Megaridis compared Equations 14.50–14.52 to both simulation data for total scattering of Mountain and Mulholland[4] and their own porous sphere model with success. We remark that Koylu and Faeth,[14] Kazakov and Frenklach[34] and Mulholland and Choi[35] have considered the

problem of the total scattering cross section for an aggregate, but the resulting expressions are more complex than those above.

14.5.2.4 Fractal Aggregate Albedo

A useful quantity is the albedo, which is the ratio of scattering to total extinction

$$\omega = \frac{C_{\text{sca}}}{(C_{\text{sca}} + C_{\text{abs}})} \tag{14.53}$$

For a particle or aggregate with a real refractive index (no imaginary part), $C_{\text{abs}} = 0$ and hence, $\omega = 1$.

For an aggregate of particles with complex refractive index, the use of Equations 14.48 and 14.50 in Equation 14.53 yields

$$\omega^{\text{agg}} = \left(1 + \frac{3}{2}\left(\frac{E(m)}{F(m)}\right) ka^{-3}\left(NG(kR_{\text{g}})\right)^{-1}\right)^{-1} \tag{14.54}$$

where $G(kR_{\text{g}})$ is given by Equation 14.52. This albedo is plotted for soot in Figure 14.8. The calculations were performed[2] for $\lambda = 500$ nm and $3(E/F)/2k_{\text{o}} = 1$, which is a typical combination for carbonaceous soot. Figure 14.8 shows that initially $\omega^{\text{agg}} \sim R_g$, but this quickly saturates near $R_g = 100$ nm. In a previous review, Equation 14.54 was shown to give a good comparison to the soot albedo data of Mulholland and Choi[35] attesting to the veracity of G as well.

14.5.2.5 The Meaning of the RDG Fractal Aggregate Approximation

Attention to the development above uncovers the meaning of the RDG Fractal Aggregate Approximation.

First, the mathematical machinery of RDG is the Fourier transform, the physical motivation of the Fourier transform is addition of waves from a source. The addition of waves from a

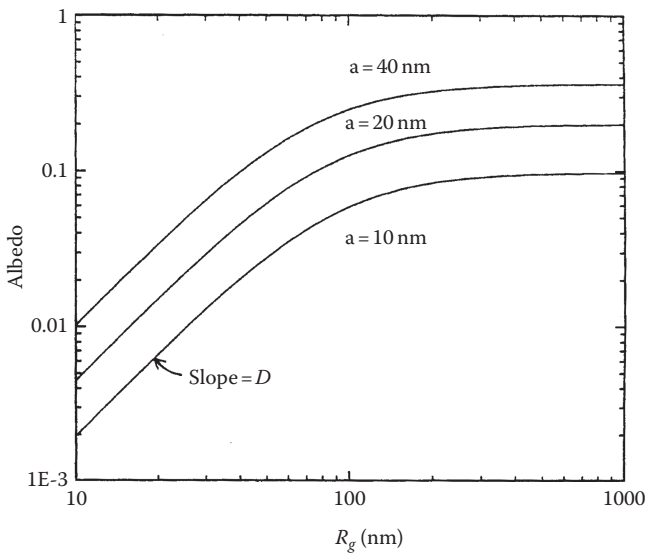

FIGURE 14.8 The albedo for a soot-like fractal aggregate calculated with Equation 14.54 with $D_f = 1.75$, $E/Fk_0 = 2/3$, $\lambda = 500$ nm and various monomer radii a. (From Sorensen, C.M. 2001. *Aerosol Sci. Tech.* 35:2648–2687. With permission.)

source is diffraction, and since we implicitly assumed the far field, Fraunhofer diffraction, a subject in sophomore physics. Simply said, RDG is diffraction from whatever object you are scattering from.

Second, in RDG fractal aggregate light-scattering theory, the electromagnetism is added at the monomer level as Rayleigh scattering. This gives a magnitude to the scattered waves that are subsequently added together via the laws of diffraction.

Third, the electromagnetism follows the diffraction sequentially; they are not convoluted together. Such convolution of the wave and electromagnetic natures of light is the complete and correct description of light's interaction with matter and is the basis for complete theories such as the Lorenz–Mie theory. It is the weak coupling between the monomers of the aggregate that allows the deconvolution of the electromagnetism and the diffraction.

14.6 SCATTERING FROM AN ENSEMBLE OF AGGREGATES

14.6.1 Effects of Polydispersity

Since aggregates are the result of aggregation, we expect that any ensemble of aggregates would be polydisperse. We need to understand the effect of polydispersity on the shape of the structure factor measured with light-scattering experiments, and with this, quantify polydispersity in terms of a measurable size distribution.[5,36] We also need to understand what the mean size we measure is, in terms of moments of the size distribution.

In general, the effective structure factor for an ensemble of aggregates can be written as

$$S_{\text{eff}}(q) = \frac{\int N^2 n(N)\, S[qR_g(N)]\, \mathrm{d}N}{\int N^2 n(N)\, \mathrm{d}N} \tag{14.55}$$

In Equation 14.55, $n(N)$ is the size distribution, that is, the number of clusters per unit volume with N monomers per cluster. One procedure to follow would be to fit data numerically using a single cluster structure factor above and an appropriate size distribution with fit variables, such as D_f and the size distribution parameters of most probable size, distribution width, and so on. Here we describe an analysis that relies on physical sense and simplicity.

We represent the single aggregate structure factor by its Rayleigh, Guinier, and power-law limits

$$S(q) = 1 \quad qR_g < 1 \tag{14.56a}$$

$$= 1 - \frac{q^2 R_g^2}{3} \quad qR_g \sim 1 \tag{14.56b}$$

$$= C\,(qR_g)^{-D_f} \quad qR_g > 1 \tag{14.56c}$$

The value of C in Equation 14.56c is 1.0 ± 0.1 for the Gaussian structure factor.[2]

The size distribution is completely described by its moments. We define the ith moment of the size distribution as

$$M_i = \int N^i n(N)\, \mathrm{d}N \tag{14.57}$$

Now substitute Equations 14.56 into 14.55 to find the ensemble equivalent of Equations 14.56

$$S_{\text{eff}}(q) = 1 \quad qR_{g,z} < 1 \tag{14.58a}$$

$$= \left(1 - \frac{q^2 R_{g,z}^2}{3}\right) \quad qR_{g,z} \sim 1 \tag{14.58b}$$

$$= C_p C(qR_{g,z})^{-D_f} \quad qR_{g,z} > 1 \tag{14.58c}$$

where $R_{g,z}$ is the z-average[28] radius of gyration given by

$$R_{g,z}^2 = a^2 k_0^{-2/D_f} \frac{M_{2+2/D}}{M_2} \tag{14.59}$$

Equation 14.58b says that a Guinier analysis of scattered light from an ensemble of particles yields the z-average radius of gyration, Equation 14.59 might be confusing at first, but consider Equation 14.1 rewritten as $\mathrm{R}_g = a\ (N/k_0)^{1/D_f}$. With this we see that the z-average radius of gyration is one which is weighted by the moments of the size distribution. Further, note that for $D_f \approx 2$ the moments are ca. M_3/M_2, high moments that stress the large N end of the size distribution. This is not surprising, because light scatters more from larger particles than smaller ones; the light-scattering process weighs the large end of the size distribution.

Notable results in Equation 14.58c are that the power law at large q retains the exponent—D_f; thus the fractal dimension measurement is unaffected by simple polydispersity (see, however, Martin and Ackerson[37]). A change occurs in that the coefficient of the power law is modified by the polydispersity of the ensemble. The modifying factor C_p is significantly different than unity, so that the use of a single cluster structure factors on scattering data would yield erroneous results. Fortunately, the result opens an opportunity to measure, to some degree, the polydispersity of the ensemble.

We call C_p the polydispersity factor; it is given by[36]

$$C_\mathrm{p} = \frac{M_1}{M_2}\left(\frac{M_{2+2/D_f}}{M_2}\right)^{D_f/2} \tag{14.60}$$

Given a size distribution, the polydispersity factor C_p can be calculated. It is well established that an aggregating system develops a self preserving, scaling distribution given by[38–40]

$$n(N) = As^{-2}\, x^{-\tau} e^{-\alpha x} \tag{14.61}$$

where A and α are constants, x is the relative size

$$x = \frac{N}{s}, \tag{14.62}$$

and s is a mean size. Notice that the size in this context is the aggregation number, N. The exponent τ is a measure of the width of the distribution with large τ implying a broad distribution. This scaling form is valid when $x > 1$, the small x form being different. Since scattering strongly weighs the large end part of the distribution, that is, $x > 1$, the small x part has little effect on the properties of scattering from an ensemble of aggregates and hence can be ignored.

The log normal distributions are frequently used in the literature. However, we have shown[41] that these distributions yield erroneous values for distribution moments higher than the second when compared to the exact scaling distribution. For the second moment and lower, the distributions

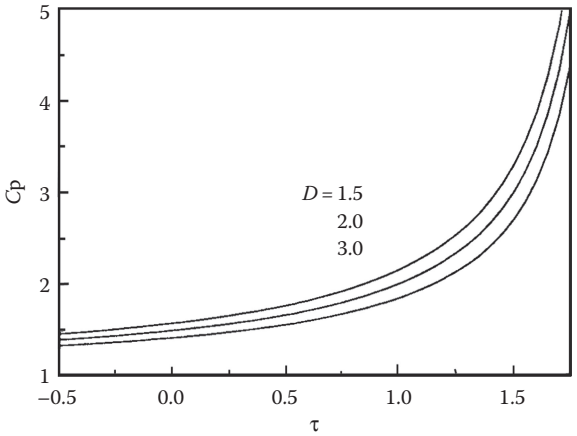

FIGURE 14.9 The polydispersity factor of Equation 14.60 plotted versus the scaling exponent τ for three different fractal dimensions. (From Sorensen, C.M. and Wang, G.M. 1999. *Phys. Rev. E* 60:7143–7148. With permission.)

agree well. Since scattering involves higher moments, such as $M_{2+2/D} \approx M_3$ for $D \approx 2$, it is erroneous to use the log normal distribution for light-scattering analysis.

In Figure 14.9, C_p is shown as a function of the width parameter τ for a variety of fractal dimensions D. In particular, for DLCA in the continuum regime it is expected and well verified that $\tau = 0$ and $D_f = 1.75$ to 1.8. From Figure 14.9 we find $C_p = 1.53$. We have applied Equation 14.60 successfully for measuring the size distribution exponent.[36]

In summary, the optical structure factor is a very capable method for yielding R_g, D_f, and the scaling distribution polydispersity exponent τ. Under the RDG approximation, the particle refractive index need not be known. If data beyond $qR_g \approx$ are not available, the D_f measurement can only be considered qualitative.

14.6.2 The Tyndall Effect

The Tyndall effect is the increased scattering as an ensemble of particles aggregates. We assume that the system neither gains nor loses particulate mass, that is, the total number of monomers (also called "primary particles") is constant, but the particles come together and form larger particles. Here we will take these larger particles as fractal aggregates. We also require no expansion or contraction of the system to maintain constant volume. Let n be the number of clusters per unit volume in the system. Then the scattered intensity has the proportionality

$$I(q) \sim nN^2 S_{\text{eff}}(q) \tag{14.63}$$

With the use of Equation 14.56, we can write

$$I(q) \sim nN^2, \quad qR_g < 1 \tag{14.64a}$$

$$I(q) \sim nN^2 (qR_g)^{-D_f}, \quad qR_g > 1. \tag{14.64b}$$

The product nN is the total number of monomers in the system, N_m, which is conserved. From Equation 14.1, $NR_g^{-D_f}$ is a constant. With these facts, Equations 14.64 become

$$I(q) \sim N_m N, \quad qR_g < 1 \tag{14.65a}$$

$$I(q) \sim N_m, \quad qR_g > 1. \tag{14.65b}$$

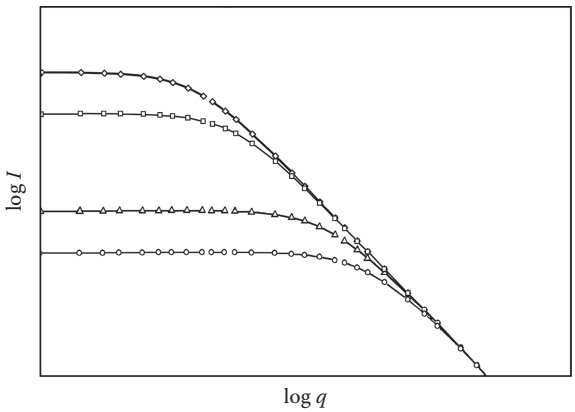

FIGURE 14.10 Sketch of the evolution with time of the scattered intensity versus q on a log–log plot as the system aggregates. The enhanced scattering in the Rayleigh regime is the Tyndall effect for fractal aggregates. (From Sorensen, C.M. 2001. *Aerosol Sci. Tech.* 35:2648–2687. With permission.)

We see that with aggregation the scattered intensity in the Rayleigh regime increases as the number of monomers in the aggregates N increases, but the power-law regime stays constant during aggregation. This behavior is sketched in Figure 14.10 and shown with an aggregating aerosol in Figure 14.11.[42]

14.7 OPTICAL PARTICLE SIZING

One of the major motivations for understanding how aggregates scatter and absorb light is to allow *in situ* light-scattering and absorption measurements of particle size, morphology, and number density. Light scattering is noninvasive, remote, and as good as or better than any other more "direct" method, such as transmission electron microscopy (TEM). Reciprocal space is just as good as real space.

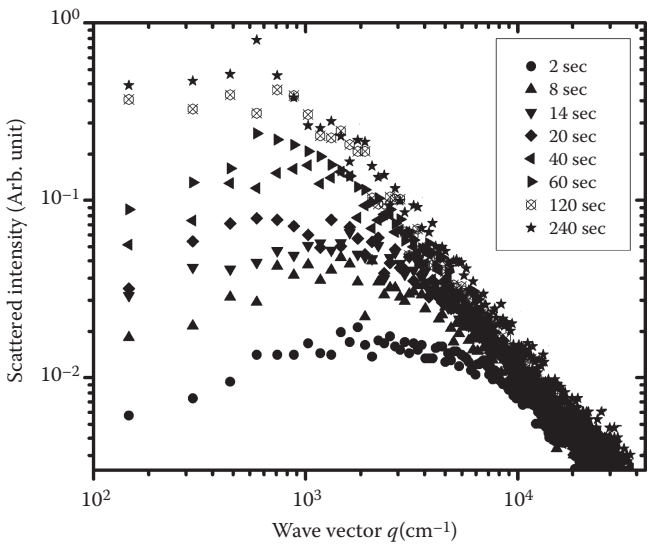

FIGURE 14.11 Experimental light-scattering data from a dense, aggregating, soot aerosol demonstrating the Tyndall effect. The legend indicates time after the aerosol was created by explosion of a fuel rich acetylene/oxygen mixture.

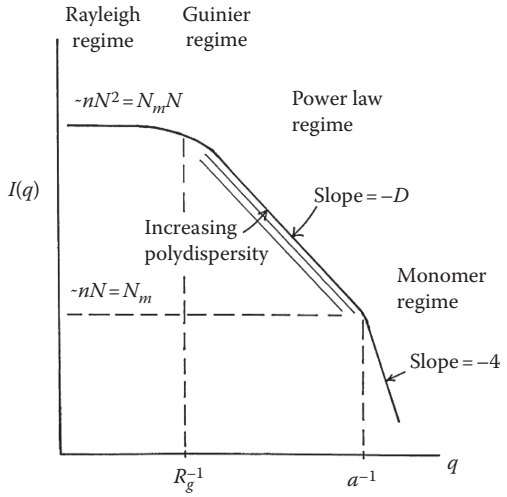

FIGURE 14.12 Double log plot of the scatter light intensity as a function of q for a group of fractal aggregates made of spherical particles of radius a with average monomer number N. The aggregates have a z-average radius of gyration of $R_{g,z}$ and a fractal dimension D_f. The group has n aggregates per unit volume and the total number of monomers in the system is $N_m = nN$. (From Sorensen, C.M. 2001. *Aerosol Sci. Tech.* 35:2648–2687. With permission.)

14.7.1 The Optical Structure Factor

Scattered intensity versus angle is the experimental method used, but the angle is best converted to q which, under the RDG approximation, is reciprocal or Fourier space of the scattering object. We call the measurement of I vs. q plotted log–log an optical structure factor analysis.[43] From the optical structure factor, one can determine the aggregate average R_g and D_f, the polydispersity of the aggregate size distribution, and the monomer size a, if short wavelengths or large a is available. These facts are outlined schematically in Figure 14.12, which is the ensemble-scattering analogue of Figure 14.7.

An example from some of our studies[2] is given in Figure 14.13 for scattering from a titania aerosol. This aerosol was created by the hydrolysis of titanium tetraisopropoxide vapor in humid air and then

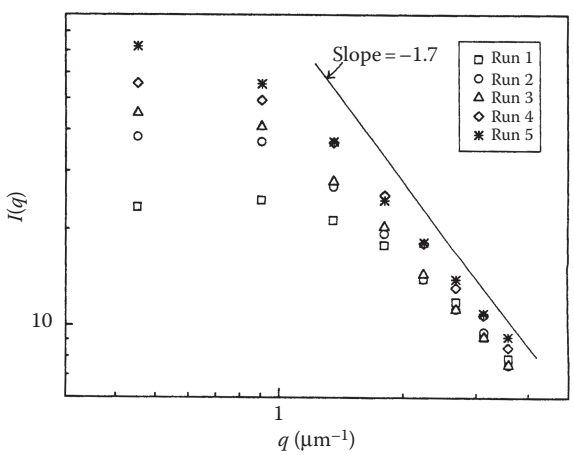

FIGURE 14.13 Optical structure factor analysis of an aggregating TiO_2 aerosol. Later times are larger run numbers.

contained in a 6 L scattering chamber. The incident light had a wavelength of 488 nm. Inspection of Figure 14.13 shows that with increasing age of the aerosol as indicated by run number, the bend in the optical structure factor where the slope of I vs. q goes from zero to negative, progresses to smaller q. A cardinal rule is that a change in slope on these log–log plots implies a length scale. In this case, the length scale is the overall aggregate size, and since $R \sim q^{-1}$, this is a direct observation, albeit qualitative, of the aggregate size increasing with time. Also seen is a significant power-law regime with a slope implying $D_f \approx 1.7$. The $I(q = 0)$ limit (the Rayleigh regime) increases with run time. This is the Tyndall effect that as a system coarsens, and it scatters more light. On the other hand, the power-law regime in Figure 14.13 approaches a constant intensity as described above.

Guinier analysis of the data in Figure 14.13 is shown in Figure 14.14. We have found this works best by inverting the Guinier result, Equation 14.58b, to

$$\frac{I(0)}{I(q)} \approx 1 + \frac{q^2 R_{g,z}^2}{3} \tag{14.66}$$

Plotting the inverse, normalized scattered intensity versus q^2 yields linear graphs with a slope equal to $R_{g,z}^2/3$.

14.8 TESTS OF THE VALIDITY OF RDG FRACTAL AGGREGATE LIGHT SCATTERING

In a previous review of this subject,[2] the author made a comprehensive analysis of work testing the validity of the RDG description of fractal aggregate scattering and absorption up to 1999. The general conclusion was that the neglect of the monomer–monomer scattering interaction, referred to as internal multiple scattering in that study, may lead to errors in the cross sections in the 10–20% range both positive and negative. For small ka, the scattering can be greater than RDG predictions. On the other hand, if the imaginary refractive index is significant, absorption can cause screening of the aggregate interior with concomitant less scattering than the RDG prediction. A fractal dimension $D_f > 2$ also causes less actual scattering analogous to the decreased scattering of spheres relative to the Rayleigh regime, once out of the Rayleigh regime. Comparison to calculations by

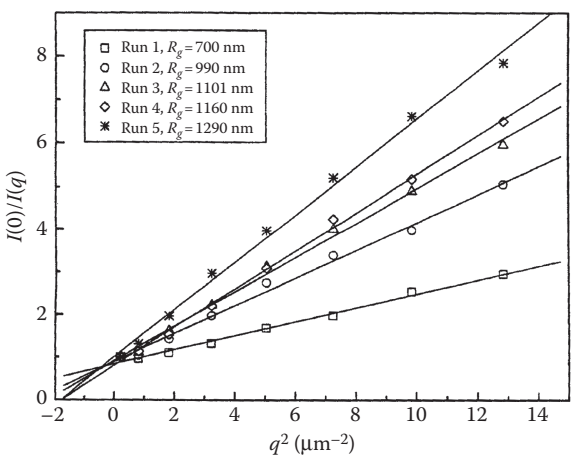

FIGURE 14.14 Titania aerosol of Figure 14.13 plotted for a Guinier analysis ala Equation 14.66. Note that the bulk of the data extend beyond the Guinier regime.

Farias et al.[44] indicated that a phase-shift parameter for fractal aggregates could be defined and RDG theory was good to 10% when

$$\rho = 2kR_g(m-1) < 3. \tag{14.67}$$

where m is the real part of the index of refraction of the monomers.

The analysis of experimental tests not only outlined all the problems in the optical measurements but also more problems in comparative measurements, most notably perturbative sampling of the aerosol and measurement of properties under the TEM. Experiments found no major discrepancies for measuring R_g, N, and D_f, but both the optical and TEM methods had significant uncertainties.

The overall conclusion of that review was that for $D_f \approx 1.78$ and ka on the order of <0.5, RDG was good to 10%.

Subsequently, Wang and Sorensen[45] tested the RDG theory with light-scattering measurements on TiO_2 and SiO_2 aerosols that aggregated to yield $D_f \approx 1.8$ aggregates. Note, that the TiO_2 has a large refractive index of 2.6. They dealt with polydisperse aerosols, measured the polydispersity with light-scattering methods, and compared scattering RDG, predicted and experimentally measured cross sections. The agreement was within the experimental errors of ca. 10%.

Chakrabarty et al.[46] compared the RDG theory predictions to data from a soot aerosol with $D_f = 1.7$. They used a tandem DMA set up to achieve a quasi-monodisperse distribution of aggregate sizes centered at a mobility radius of 400 nm. This eliminated the problem of the size distribution and the higher moment weighting of light scattering. Agreement between theory and experiment was good up to 10–25% depending on the value of the soot refractive index, another notorious experimental uncertainty.

Van-Hulle et al.[47] compared the RDG results to both the discrete dipole approximation (DDA)[48,49] and the "rigorous solution" (RS) of Xu et al.[50] Their theoretical aggregates were soot with $D_f = 1.8$

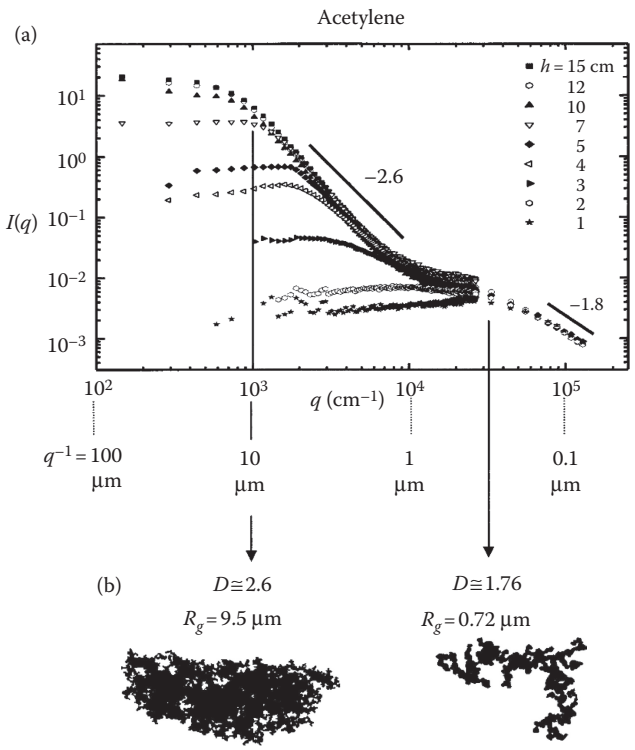

FIGURER 14.15 Optical structure factor and TEM pictures of soot superaggregates in and obtained from a laminar diffusion acetylene flame.

with $ka = 0.15$ and $N = 64$, 128, and 256. DDA and RS agreed well with each other for both absorption and total scattering cross sections and with RDG for absorption cross sections. However, RDG was 60 to 120% in error for the scattering.

Yon et al.[51] compared the RDG theory to more exact calculations that included monomer–monomer electromagnetic interactions, that is, internal multiple scattering. They created $D_f = 1.8$ aggregates for the calculations with $N = 64$, 128, and 256 and varied the monomer size up to $ka = 0.9$. They found that for small ka the scattering at $q = 0$ was ca. 5% greater than predicted by RDG (see above) but fell to as much as 20% smaller at the largest ka. The absorption cross section was good up to 10%. The predictions of total scattering, Equations 14.50–14.52, were verified but the best fit to RDG required $D_f = 2.24$. Most unexpected, however, was that the large qR_g regime yielded fractal dimensions of 2.34 ± 0.15 instead of the fractal dimension of 1.8. These large values of D_f were not explained and stand in strong contrast to many experiments that have yielded the correct fractal dimension when compared to nonscattering methods.

Finally, I will stretch the envelope a bit. Studies in our labs over the past several years[15–17] have uncovered the existence of soot superaggregates; aggregates of one morphology composed of aggregates of another morphology. Figure 14.15 shows both optical structure factor measurements and TEM pictures of soot from a heavily sooting, laminar diffusion, acetylene flame. Both indicate that the soot has a fractal dimension of $D_f = 2.6$ for length scales in the range of ca. 1–10 μm and a fractal dimension of $D_f = 1.8$ for submicron scales. We ask: how is it that the analysis of the light-scattering data with RDG scattering theory agrees well with the TEM measurements? Does the RDG theory work for 10 μm, $D_f = 2.6$ superaggregates?

We conclude in much the same way we did in 1999. It appears that the RDG formulation of scattering and absorption by fractal aggregates is accurate to ca. 10%.

14.9 CONCLUSION

The fundamental aspects of RDG fractal aggregate light scattering have been laid out above in what the author hopes is a straightforward and accessible manner. Despite the author's failings, the theory's simplicity speaks for itself. Although approximations that allow this simplicity cause concern for the theory's validity, the theory has proven extremely useful in describing the otherwise complex problem of how fractal aggregates scatter and absorb light. Its use for the diagnostics of aerosols (and colloids) is no less suspect than many other alternative diagnostics. Finally, I will end in the same way I did in 2001 with my first review of this subject[2] by reminding the reader that the scattering wave vector q (not θ) is the physically motivated independent variable for all scattering experiments. Moreover, this is by and large a geometric universe and hence, logarithmic axes more readily uncover features in data than linear ones. Plot your data double log, scattered intensity versus q.

ACKNOWLEDGMENTS

Since 2001 my work has benefited from the pleasant and stimulating collaboration with my students M. Beavers, M. Berg, R. Dhaudhabel, D. Fry, C. Gerving, S.E. Gilbertson, J. Hubbard, W.G. Kim, T. Mokhtari, F. Pierce, and R. Pyle and my good friend and colleague Amit Chakrabarti. My work has been supported by NSF and NASA.

REFERENCES

1. Forrest, S.R. and Witten, T.A. 1979. Long-range correlations in smoke-particle aggregates. *J. Phys. A* 12:L109–L117.
2. Sorensen, C.M. 2001. Light scattering from fractal aggregates. A review. *Aerosol Sci. Tech.* 35:2648–2687.
3. Mandelbrot, B. 1983. *The Fractal Geometry of Nature*. Freeman, San Francisco, CA.

4. Mountain, R.D. and Mulholland, G.W. 1988. Light-scattering from simulated smoke agglomerates. *Langmuir* 4:1321–1326.
5. Nicolai, T., Durand, D., and Gimel, J.-C. 1994. Static structure factor of dilute solutions of polydisperse fractal aggregates. *Phys. Rev. B* 50:16357–16363.
6. Cai, J., Lu, N., and Sorensen, C.M. 1995. Analysis of fractal cluster morphology parameters: Structural coefficient and density autocorrelation function cutoff. *J. Colloid Interface Sci.* 171: 470–473.
7. Lattuada, M., Wu, H., and Morbidelli, M. 2003. A simple model for the structure of fractal aggregates. *J. Colloid Interface Sci.* 268:106–120.
8. Meakin, P. 1983. Formation of fractal clusters and networks by irreversible diffusion-limited aggregation, *Phys. Rev. Lett.* 51:1119–1122.
9. Kolb, M., Botet, R., and Jullien, R. 1983. Scaling of kinetically growing clusters. *Phys. Rev. Lett.* 51:1123–1126.
10. Jullien, R. and Botet, R. 1987. *Aggregation and Fractal Aggregates*. World Scientific, Singapore.
11. Meakin, P., Fractal Aggregates 1988. *Adv. Colloid & Interface Sci.* 28:249–331.
12. Sorensen, C.M. and Roberts, G. 1997. The prefactor of fractal aggregates. *J. Colloid Interface Sci.* 186:447–452.
13. Sorensen, C.M. and Oh, C. 1998. Divine proportion shape invariance and the fractal nature of aggregates. *Phys. Rev.* E58:7545–7548.
14. Koylu, U.O. and Faeth, G.M. 1995. Optical properties of overfire soot in buoyant turbulent diffusion flames at long residence times. *Trans. ASME* 116:152–159.
15. Sorensen, C.M., Kim, W., Fry, D., and Chakrabarti, A. 2003. Observation of soot superaggregates with a fractal dimension of 2.6 in laminar acetylene/air diffusion flames. *Langmuir* 19:7560–7563.
16. Kim, W., Sorensen, C.M., and Chakrabarti, A. 2004. Universal occurrence of soot aggregates with a fractal dimension of 2.6 in heavily sooting laminar diffusion flames. *Langmuir* 20:3969–3973.
17. Kim, W., Sorensen, C.M., Fry, D., and Chakrabarti, A. 2006. Soot aggregates, superaggregates and gel-like networks in laminar diffusion flames. *J. Aerosol Sci.* 37:386–401.
18. van de Hulst, H.C. 1981. *Light Scattering by Small Particles*. Dover, New York, NY.
19. Kerker, M. 1969. *The Scattering of Light and Other Electromagnetic Radiation.* Academic Press, New York, NY.
20. Bohren, C.F. and Huffman, D.R. 1983. *Absorption and Scattering of Light by Small Particles.* John Wiley & Sons, New York, NY.
21. Sorensen, C.M. and Fischbach, D.E. 2000. Patterns in Mie scattering. *Opt. Commun.* 173:145–153.
22. Sorensen, C.M. and Shi, D. 2000. Guinier analysis for homogeneous dielectric spheres of arbitrary size. *Opt. Commun.* 178:31–36.
23. Sorensen, C.M. and Shi, D. 2002. Patterns in the ripple structure in Mie scattering. *JOSA* 19:122–125.
24. Berg, M.J., Sorensen, C.M., and Chakrabarti, A. 2005. Patterns in Mie scattering: Evolution when normalized by the Rayleigh cross section. *Appl. Opt.* 44:7487–7493.
25. Oh, C. and Sorensen, C.M. 1999. Scaling approach for the structure factor of a generalized system of scatterers. *J. Nanopart. Res.* 1:369–377.
26. Guinier, A., Fournet, G., Walker, C.B., and Yudowitch, K.L. 1955. *Small Angle Scattering of X-Rays*. Wiley, New York, NY.
27. Teixeira, J. 1986. Experimental methods for studying fractal aggregates, in *On Growth and Form, Fractal and Non-Fractal Patterns in Physics*, H.E. Stanley and N. Ostrowski, (Eds), Nijhoff, Dordrecht. 145–165.
28. Martin, J.E. and Hurd, A.J. 1987. Scattering from fractals. *J. Appl. Cryst.* 20:61–78.
29. Fisher, M.E. and Burford, R.J. 1967. Theory of critical-point scattering and correlations I. The Ising model. *Phys. Rev.* 156:583–622.
30. Sorensen, C.M., Cai, J., and Lu, N. 1992. Test of static structure factors for describing light scattering from fractal soot aggregates. *Langmuir* 8:2064–2069.
31. Porod, G. 1951. Die Röntgonkleinwinkelstreuung von Dichtgepacken Kolloiden Systemen. *Kolloid Z.* 124:83–114.
32. Jullien, R. 1992. From Guinier to fractals. *J. Phys. I* (France) 2:759–770.
33. Dobbins, R.A. and Megaridis, C.M. 1991. Absorption and scattering of light by polydisperse aggregates. *Appl. Opt.* 30:4747–4754.
34. Kazakov, A. and Frenklach, M. 1998. Dynamic modeling of soot particle coagulation and aggregation; implementation with the method of moments and application to high-pressure laminar premixed flames. *Combust. Flame* 114:484–501.

35. Mulholland, G.W. and Choi, M.Y. 1998. Measurement of the mass specific extinction coefficient for acetylene and ethene smoke using the large agglomerate optics facility, *Twenty-Seventh Symposium (International) on Combustion*, The Combustion Institute, 1515–1522.
36. Sorensen, C.M. and Wang, G.M. 1999. Size distribution effect on the power law regime of the structure factor of fractal aggregates. *Phys. Rev. E* 60:7143–7148.
37. Martin, J.E. and Ackerson, B.J. 1985. Static and dynamic light scattering by fractals. *Phys. Rev.* A31:1180–1182.
38. Friedlander, S.K. and Wang, C.S. 1966. The self-preserving particle size distribution for coagulation by Brownian motion. *J. Colloid Interface Sci.* 22:126–132.
39. Wang, C.S. and Friedlander, S.K. 1967. The self-preserving particle size distribution for coagulation by Brownian motion. *Jour. Coll. Interface Sci.* 24:170–179.
40. van Dongen, P.G.J. and Ernst, M.H. 1985. Dynamic scaling in kinetics of clustering. *Phys. Rev. Lett.* 54:1396–1399.
41. Sorensen, C.M., Cai, J., and Lu, N. 1992. Light-scattering measurements of monomer size, monomers per aggregate, and fractal dimension for soot aggregates in flames. *Appl. Opt.* 31:6547–6557.
42. Dhaubhadel, R., Chakrabarti, A., and Sorensen, C.M. 2009. Light scattering study of aggregation kinetics in dense, gelling aerosols. *Aerosol Sci. Technol.* 43:1053–1062.
43. Gangopadhyay, S., Elminyawi, I., and Sorensen, C.M. 1991. Optical structure factor measurements for soot particles in a premixed flame. *Appl. Opt.* 30:4859–4864.
44. Farias, T.L., Koylu, U.O., and Carvalho, M.G. 1996. Range of validity of the Rayleigh–Debye–Gans theory for optics of fractal aggregates. *Appl. Opt.* 35:6560–6567.
45. Wang, G.M. and Sorensen, C.M. 2002. Experimental test of the Rayleigh–Debye–Gans theory for light scattering by fractal aggregates. *Appl. Opt.* 41:4645–4651.
46. Chakrabarti, R.K., Moosmuller, H., Arnott, W.P., Garro, M.A., Slowik, J.G., Cross, E.S., Han, J.-H., Davidovits, P., Onasch, T.B., and Worsnop, D.R. 2007. Light scattering and absorption by fractal-like carbonaceous chain aggregates: Comparison of theories and experiment. *Appl. Opt.* 46, 6990–7006.
47. Van-Hulle, P., Weill, M.-E., Talbaut, M., and Coppalle, A. 2002. Comparison of numerical studies characterizing optical properties of soot aggregates for improved EXSCA measurements. *Part. Part. Syst. Charact.* 19:47–57.
48. Draine, B.T. 1988. The discrete-dipole approximation and its application to interstellar graphite grains. *Astrophys.* 333:848–872.
49. Draine, B.T. and Flatau, P.J. 1994. Discrete-dipole approximation for scattering calculations. *J. Opt. Soc. Am.* A. 11:1491–1499.
50. Xu, Y.L. and Gustafson, A.S. 1999. Comparison between multisphere light-scattering calculations. Rigorous solution and discrete dipole approximation. *Astrophys. J.* 513:894–909, and references therein.
51. Yon, J., Roze, C., Girasole, T., Coppalle, A., and Mees, L. 2008. Extension of RDG-FA for scattering prediction of aggregates of soot taking into account interactions of large monomers. *Part. Part. Syst. Charact.* 25:54–67.